Theory and experiment on the optical properties of $CrSi_2$

V. Bellani, G. Guizzetti, F. Marabelli, and A. Piaggi
Dipartimento di Fisica "A. Volta," Università degli Studi di Pavia, Via Bassi 6, I-27100 Pavia, Italy

A. Borghesi and F. Nava
Dipartimento di Fisica, Università degli Studi di Modena, Via Campi 213/A, I-41100 Modena, Italy

V. N. Antonov,* Vl. N. Antonov,* O. Jepsen, and O. K. Andersen
Max-Planck-Institut für Festkörperforschung, Stuttgart 80, Federal Republic of Germany

V. V. Nemoshkalenko
Institute of Metal Physics, Vernadskogo 36, 252142 Kiev, Ukraine
(Received 3 February 1992; revised manuscript received 10 June 1992)

The optical properties of $CrSi_2$, both in polycrystalline and single-crystal form, were investigated between 0.01 and 5 eV. The dielectric functions were determined by different methods: Kramers-Kronig transformations of the near-normal reflectivity over the whole spectral range; direct measurement by spectroscopic ellipsometry from 1.4 to 5 eV; numerical inversion of the reflectance from two films with different thickness. The main difference between thin-film and single-crystal data is the presence, in the latter, of a strong free-carrier response, preventing the determination of the intrinsic absorption edge (interband optical gap). Moreover, the optical properties of $CrSi_2$ were calculated within the local-density approximation using the semirelativistic linear-muffin-tin-orbital method. The band structure, the l-projected densities of states, the complex dielectric function, and the optical reflectivity were obtained in the energy range from 0 to 5 eV. The theoretical calculations are compared with the experimental data.

I. INTRODUCTION

Transition-metal silicides (TMS) have been intensively studied, from both fundamental and applied points of view, due to their important applications in very large integrated-circuit technology as metallic materials for gate electrodes and interconnections.[1] Only four TMS, i.e., $CrSi_2$, β-$FeSi_2$, $MnSi_2$, and $ReSi_2$, were found to be semiconductors, with energy gaps in the 0.1–0.9-eV energy range.[1] The main applicative interest of these semiconductors is connected (i) with a large thermoelectric power, usable in the thermoelectric conversion, and (ii) with their potential application as optoelectronic devices (infrared detectors and sources, electro-optic interconnects, etc.). Moreover, it is known that they can grow epitaxially to a certain extent on silicon,[2] so that they have some suitable characteristics in comparison with polycrystalline materials.

$CrSi_2$ has the lowest growth temperature and is the most widely studied and characterized semiconducting silicide. Nevertheless, only recently optical studies on well-characterized $CrSi_2$ thin films have provided convincing evidence for the semiconducting character. These measurements have shown that $CrSi_2$ exhibits an indirect band gap of about 0.35 eV.[3]

The optical spectra of solids contain a wealth of information about their electronic structure, but for compounds with complex crystal structure it is very difficult to interpret the measured optical properties without knowledge of their energy-band structure.

The previous energy-band calculations of $CrSi_2$ were based on the extended-Huckel-theory.[4] This semiempirical approach predicts semimetallic properties as a result of a slight band overlap ($\sim$0.1 eV) near the M point in the Brillouin zone (BZ).

On the other hand, recent results of linear augmented-plane-wave band calculations (LAPW) (Refs. 5 and 6) for hexagonal $CrSi_2$, carried out using the local-density approximation (LDA) to density-functional theory,[7] confirm that this compound is an indirect-gap semiconductor. The calculated indirect gap of 0.30 eV is in excellent agreement with the measured optical value of 0.35 eV. This agreement of the calculated LDA band gap with the experimental value may suggest that the well-known "band-gap" problem[8] is less severe in $CrSi_2$ than in typical tetrahedral s-p bonded semiconductors due to the similarity of Cr $3d$ orbital characteristics of the states on both sides of the gap. Also, it was shown[5] that the calculated gap is very sensitive to the local Cr-Si coordination geometry. The energy gap varies by 0.1 eV for Si position changes of $0.01c$.

The results for the electronic structure and optical properties of $CrSi_2$ obtained from self-consistent augmented-spherical-wave (ASW) calculations have been presented in Ref. 9. The ASW basis set included $4s$, $4p$, and $3d$ orbitals on Cr, and $3s$, $3p$, and $3d$ orbitals on

Si. The calculated indirect and direct gaps are 0.21 and 0.39 eV, respectively. The real $\epsilon_1(\omega)$ and imaginary $\epsilon_2(\omega)$ parts of the dielectric function, as well as the absorption coefficient, were calculated, but a comparison between the theory and the experiment was made only for the absorption coefficient in the small energy region between 0.1 and 0.9 eV.

The aim of the present work is a direct comparison of the measured optical properties of $CrSi_2$ [reflectivity $R(\omega)$, $\epsilon_1(\omega)$ and $\epsilon_2(\omega)$] with the calculated optical spectra, in the more extended region from 0.01 to 5 eV. The theoretical spectra were obtained from the electronic energy bands and wave functions using the LDA.[10] The interpretation of the $\epsilon_2(\omega)$ in terms of the interband transitions and an investigation of the optical anisotropy are also presented.

II. EXPERIMENTAL AND COMPUTATIONAL DETAILS

A. Experiment

We used polycrystalline samples grown by two different methods. (i) Amorphous thin films of Cr-Si alloys (AL) were prepared by coevaporation of Cr and Si in a double electron-gun evaporation system. Typical deposition rates were 0.6 nm/sec for Cr and 1 nm/sec for Si. The background pressure during evaporation was 2×20^{-7} Torr. (ii) Amorphous Si film, 200–400 nm thick, and Cr film, 50–100 nm thick, were evaporated consecutively at rates of 2.5 and 5 nm/sec, respectively, forming a bilayer Si/Cr sample (BL). The background pressure was maintained at 4×10^{-7} Torr. The thickness ratio of Cr and Si was chosen to be $\frac{1}{2}$ in order to form stoichiometric $CrSi_2$ films.

Both the AL and BL films were deposited at room temperature on oxidized single-crystal Si wafers, in order to perform resistivity and Hall voltage measurements too. The samples were then annealed at 900 °C for 1 h in high vacuum (4×10^{-7} Torr) to obtain crystallization. To reduce the intake of impurities upon heat treatment, the surface of the films was covered with a clean outgassed quartz wafer during the furnace annealing.

The phase identification and the extent of recrystallization were determined by glancing incidence x-ray diffraction using a Seema-Bohlin diffractometer: complete crystallization was found. Rutherford backscattering spectroscopy (RBS) with a 2-MeV $^4He^+$ ion beam was used for depth composition analysis and for determining the film thickness (with an uncertainty of ±10 nm). Finally, Auger electron spectroscopy showed that the oxygen and carbon levels in the films were below the detection limit (0.1%).

From the measurements, on the same samples, of the electrical resistivity ρ and the Hall coefficient R_H versus the temperature T it was found[11] that $CrSi_2$ is a p-type semiconductor with an energy gap of the order of 0.27 ± 0.01 eV and a room-temperature hole concentration p ranging from 4 to 7×10^{19} cm^{-3}.

The single-crystal sample was grown by chemical transport reactions.

Near-normal incidence reflectance (R) measurements at room temperature have been performed in the energy range from 0.01 to 0.5 eV by a Fourier transform spectrometer Bruker IFS 113v, with an instrumental resolution of 0.5 meV and with a gold mirror as reference. Between 0.5 and 6 eV the $CrSi_2$ reflectance has been measured with a Perkin Elmer 330 spectrophotometer. An Al mirror, whose absolute reflectivity was previously measured, was used as reference. In the overlapping spectral regions, the reflectivity values obtained by different spectrometers agreed within the limits of experimental uncertainty.

Moreover, the optical response from 1.4 to 4.9 eV was studied by directly measuring the refraction index n and the extinction coefficient k with an ellipsometer Sopra MOSS ES4G. The R spectrum derived from ellipsometric data showed good agreement with the directly measured reflectivity in the range of energies where the spectra overlap.

B. Computational details

$CrSi_2$ crystallizes in the hexagonal C40 structure with three $CrSi_2$ formula units per unit cell. The arrangement of the individual atoms in the primitive cell is shown in Fig. 1(a). The space group for this C40 structure is $P6_222$ (D_6^4), which is nonsymmorphic, containing nonprimitive translations ($\tau = c/3$ and $2c/3$) which interchange individual $CrSi_2$ layers. The corresponding BZ is shown in Fig. 1(b), where the symmetry points and lines are labeled in accordance with the standard notations of Ref. 12. The lattice constants are a=4.431 and c=6.364 Å.[13,14]

A detailed description of the linear-muffin-tin-orbital (LMTO) method, and the atomic-spheres-approximation (ASA), which we have used, including its application to the electronic structure of compounds, is given elsewere.[15,16] The present calculations were carried out in a semirelativistic approach and with basis functions including angular momenta up to l=3 for chromium and l=2 for silicon. The inclusion of the Cr f orbitals (which were not included in Ref. 9) does not influence the energy dispersion curves $E_n^{\mathbf{k}}$, but the f states are very important for the calculated optical properties because usually the $d \rightarrow f$ oscillator strengths are much larger than the $p \rightarrow d$ and $s \rightarrow p$ ones. The "frozen-core" approximation was adopted and the core charge densities were evaluated from the solutions of the Dirac equation for free atoms.

Exchange and correlation contributions to both atomic and crystalline potentials have been included through the density-functional description in the LDA of Barth-Hedin.[10] The $\mathbf{k}$-integrated functions have been evaluated by the tetrahedron method[17] on a grid of 196 $\mathbf{k}$ points in the irreducible part of the Brillouin zone (BZ).

The linear response of a system to an external electromagnetic field with small wave vector is determined by the imaginary part $\epsilon_2(\omega)$ of the dielectric function $\tilde{\epsilon}(\omega) = \epsilon_1(\omega) + i\epsilon_2(\omega)$. We have calculated the dielectric function for frequencies well above those of the phonons and therefore considered only electronic excitations. For these we used the random-phase approximation and ne-

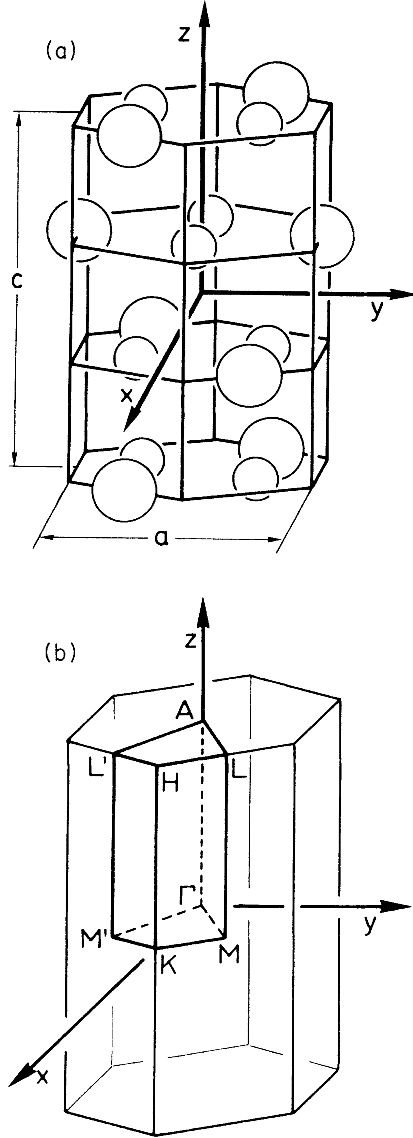

FIG. 1. (a) Primitive unit cell for hexagonal C40 structure of $CrSi_2$. Large spheres correspond to Cr atoms, small spheres correspond to silicon atoms. (b) The corresponding Brillouin zone.

glected local-field and finite lifetime effects.[18] The dielectric function is a tensor but by an appropriate choice of the principal axes we could diagonalize it and restrict our considerations to the diagonal matrix elements $\tilde{\epsilon}^{\nu\nu}(\omega)$, with $\nu = x, y, z$. The interband contribution to $\epsilon_2(\omega)$ is given by

$$\epsilon_2^{\nu\nu}(\omega) = \frac{8\pi^2 e^2}{m^2\omega^2} \sum_n^{\text{unocc}} \sum_{n'}^{\text{occ}} \int_{\text{BZ}} |\text{P}_{nn'}^{\nu}(\mathbf{k})|^2 \times \delta(E_n^{\mathbf{k}} - E_{n'}^{\mathbf{k}} - \hbar\omega)\frac{d^3k}{(2\pi)^3}, \tag{1}$$

where $\text{P}_{nn'}^{\nu}(\mathbf{k})$ is the projection of the momentum matrix elements (MME) $\mathbf{P}_{nn'}(\mathbf{k})$ along the ν direction of the electric field $\mathbf{E}$. $E_n^{\mathbf{k}}$ are the one-electron energies.

After having evaluated (1) we calculated the interband contribution to the real part of dielectric function $\epsilon_1(\omega)$ from the Kramers-Kronig (KK) relation:

$$\epsilon_1(\omega) = 1 + \frac{2}{\pi} P \int_0^\infty \frac{\epsilon_2(\omega')\omega' d\omega'}{\omega'^2 - \omega^2}, \tag{2}$$

where P stands for principal value. Finally, we obtained the total complex dielectric function by adding the intraband contribution. We neglected this contribution to $\epsilon_2(\omega)$ according to the perfect crystal approximation (the defects and lattice oscillations are absent). The intraband contribution to $\epsilon_1(\omega)$ is given by

$$\epsilon_1^{\nu\nu}(\omega)|_{\text{intra}} = 1 - \frac{(\omega_p^{\nu\nu})^2}{\omega^2}, \tag{3}$$

where the squared plasma frequency is given by

$$(\omega_p^{\nu\nu})^2 = \left(\frac{e}{\pi\hbar}\right)^2 \sum_n \int_{\text{BZ}} \left(\frac{\partial E_n^{\mathbf{k}}}{\partial k^\nu}\right)^2 \delta(E_n^{\mathbf{k}} - E_F) d^3k. \tag{4}$$

We calculated the refraction index $n(\omega)$, the extinction coefficient $k(\omega)$, and the reflectivity $R(\omega)$ using Eqs. (1)–(4) and the following relations:

$$\tilde{n}(\omega) = n(\omega) + ik(\omega) = \sqrt{\tilde{\epsilon}(\omega)}, \tag{5}$$

$$R(\omega) = \left|\frac{\sqrt{\tilde{\epsilon}(\omega)} - 1}{\sqrt{\tilde{\epsilon}(\omega)} + 1}\right|^2. \tag{6}$$

III. RESULTS

A. Optical response of $CrSi_2$

The reflectance R of the $CrSi_2$ polycrystalline films was measured for different thicknesses. No substantial difference was found between samples of type AL and BL. The data for two different thicknesses (150 and 197 nm) are presented in Fig. 2 in the energy range from 0.06 to 1.2 eV (at energies higher than 1.2 eV the reflectances tend to coincide). The SiO_2 thicknesses were 750 and 500 nm, respectively. It should be noted that the peak in R near 0.13 eV in both spectra is due to a vibrational absorption in SiO_2.

We observe that interference fringes appear; their spacing decreases for increasing film thickness: this gives direct evidence that $CrSi_2$ is transparent (or partially transparent) in the spectral region examined. Our previous work on the far-infrared response of $CrSi_2$ (Ref. 19) showed that between 100 and 700 cm^{-1} (0.0124 and 0.0868 eV, respectively) it is fully transparent, except for five strong peaks both in the reflectance and transmittance spectra, attributed to IR-active vibrational modes. No free-carrier behavior was detected down to 100 cm^{-1}. We may therefore infer that $CrSi_2$ is a narrow-gap semi-

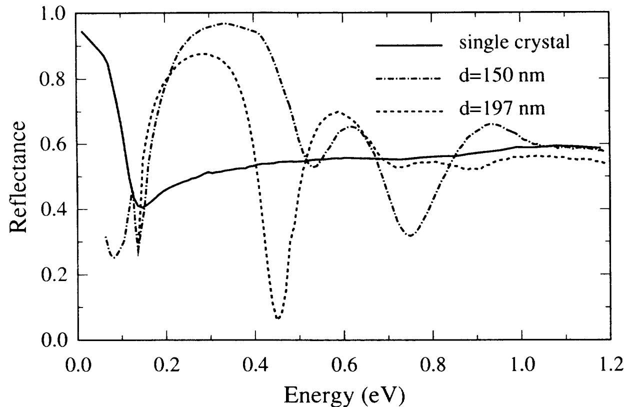

FIG. 2. Reflectance of $CrSi_2$ thin films with different thicknesses d in the energy region from 0.06 to 1.2 eV. The full line is the reflectivity of $CrSi_2$ single crystal.

conductor, in agreement with electrical transport measurements.

Bost and Mahan[3] measured the optical functions of $CrSi_2$ polycrystalline films between 0.1 and 0.8 eV. They observed a strong increase in the reflectance and a strong decrease in the transmittance at the lowest energies. On the basis of the absorption coefficient analysis they argued that this was due to free-carrier absorption. In contrast to this, our measurements provide direct evidence that the transparency region extends down to 0.01 eV, with no trace of free-carrier contribution to the optical response. This may be attributed to a better quality of our films.

The unpolarized reflectance R of the single-crystal sample is also shown in Fig. 2, in the energy range between 0.01 and 1.2 eV. Figure 3 presents R of both polycrystalline and single-crystal samples in a wide energy range up to 5 eV. The single-crystal spectrum exhibits metallic character at the lowest energies: R starts from $\sim$90% at 0.01 eV, then it rapidly decreases with increasing energy, reaching a minimum near 0.15 eV. At higher energies R rises again, showing two shoulders near 0.5 and 1.1 eV. The low-energy behavior may be ascribed to a high-impurity concentration, determining the strong free-carrier response. In fact, we observed that the impurity-related optical response also reduces the intensity of the far-infrared vibrational peaks substantially, when measurements on the polycrystalline samples were carried out.[19] In the case of single crystals, these peaks appear as much less pronounced structures superimposed on a broad Drude-like high-reflectivity plateau.

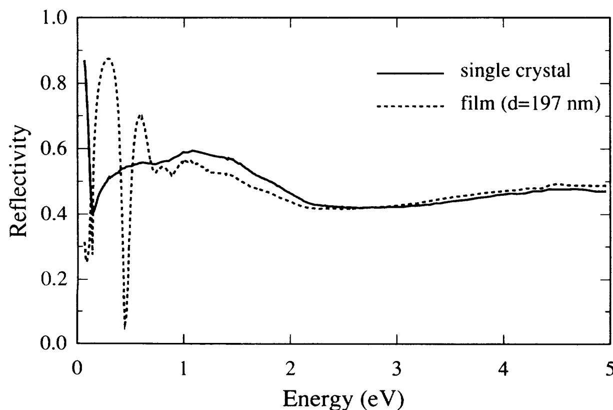

FIG. 3. Reflectivity of $CrSi_2$ single crystal and film (d=197 nm) in the wide energy range from 0.01 to 5 eV.

We start from the analysis of the interference fringes region in polycrystalline $CrSi_2$. Due to the multilayer structure of the samples ($CrSi_22/SiO_2/Si$) it was necessary to account for the contributions of the different interfaces to the multireflection process. First, we tried to solve numerically the equations in n and k giving the reflectance for two different $CrSi_2$ thicknesses. A simple method to obtain the reflectance of a multilayer system is the "matrix method,"[20] which gives a recurrence relation between the incident electric field and the field reflected by a system of N films (for an application to silicide films, see Ref. 21).

The back surface of substrates used for the R measurements was rough enough to scatter light coming from the $CrSi_22/SiO_2$ system in all directions, so that we can consider the Si film as an infinite substrate. Moreover, the thickness of each layer was known from RBS, and the optical functions of amorphous SiO_2 and crystalline Si were taken from the literature.[22,23]

The two equations $R(n,k,d_i) = R_{\rm expt}(d_i)$, where d_i (i=1,2) is the silicide thickness and $R_{\rm expt}$ is the measured reflectance, cannot be solved analytically. Several graphical methods have been proposed. In the best one a small number of contour graphs is used for a rough estimate of the initial values of n and k which are then used as the starting values in a computer search routine.[24,25] We expanded R to first order in n and k, and we obtained a system of two linear equations, using two different thicknesses. Then, the solutions were found by an iterative method using the values of n and k estimated by a graphical method as tentative initial values.

It should, however, be kept in mind that this procedure is based on the assumption of having an ideal geometrical and structural multilayer, i.e., the interfaces are considered sharp, flat, and parallel, and each layer is assumed homogeneous, with a well-defined complex refractive index. These assumptions are not fulfilled in real samples, where structural imperfections, such as nonplanarity of the interfaces, and transition regions of not-well-defined composition, are present. As a consequence, the numerical treatment may lead to unphysical results and anomalous dispersions in n and k. To avoid this we imposed the restriction that (i) the nonphysical singularities mentioned above were rejected and (ii) n and k satisfied the Kramers-Kronig relations. We also checked the influence of the silicide and the SiO_2 thickness on the interference spacings. We found that within the experimental uncertainty the thicknesses which reproduce the experimental fringes well were in agreement with those measured by RBS.

In Fig. 4 we present the resulting optical functions for polycrystalline $CrSi_2$. Between 1.4 and 5 eV (the strong

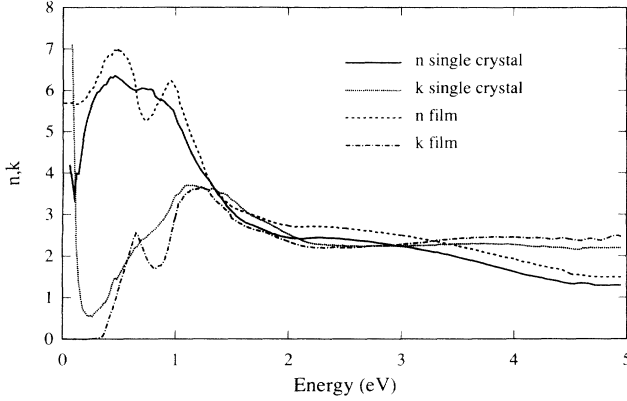

FIG. 4. Real part n and imaginary part k of the complex refractive index of $CrSi_2$ both in single crystalline and polycrystalline (thin-film) forms.

absorption region) the curves were obtained directly by ellipsometry, because the $CrSi_2$ film can be considered as bulk in this spectral region. The refraction index starts from a high value (~ 5.7) at the lowest energies, then exhibits a broad maximum near 0.5 eV and a second peak at 0.98 eV; beyond 2 eV n is nearly constant. The extinction coefficient starts increasing from zero near 0.36 eV, reaching a maximum at 0.67 eV. It is worth noting that for energies lower than 0.36 eV the accurate quantitative evaluation of k is limited by the intrinsic uncertainty of our indirect method. A stronger maximum appears at 1.2 eV, followed by a region of high k values with no appreciable structure. A comparison with the n and k curves obtained by Bost and Mahan[3] in the energy range from 0.1 to 0.8 eV is interesting. They found a broad maximum for n, and a continuous increase of k with increasing energy. Our results, on the contrary, clearly indicate that the decreasing of n towards the minimum near 0.74 eV is connected with the k structure at 0.67 eV. We emphasize that this behavior is the only one which satisfies the KK relations.

The measured far-infrared reflectance of $CrSi_2$ films reaches $\sim$ 40% at 0.01 eV.[19] As a check, we calculated R by the matrix method, using the reasonable values $n \sim 5.7$ and $k = 0$ for the silicide optical constants (see Fig. 4). We obtained $R \sim 30\%$. No appreciable variation was obtained by modifying n in order to account for the low-energy contribution of the far-infrared vibrational peaks. To explain this discrepancy, we recall that the Drude dielectric function $\tilde{\epsilon}_{\text{intra}}$ of a free-carrier gas is given by

$$\tilde{\epsilon}(\omega)_{\text{intra}} = \epsilon_{\infty} - \frac{\omega_p^2}{\omega(\omega + i\gamma)}, \tag{7}$$

where ϵ_{∞} is the high-frequency dielectric constant, ω_p is the free-carrier plasma frequency, and γ is a damping parameter, related to the scattering time τ by $\gamma = 1/\tau$.

We calculated the optical response of the $CrSi_2$ free-carrier gas by Eq. (7), considering that (i) typical scattering times for silicides range from 10^{-14} to 5×10^{-15} sec (Ref. 26); (ii) the effective mass of the $CrSi_2$ free carriers (holes) has been evaluated to be $\sim m_e$ (where m_e is the electron mass); (iii) electrical transport measurements on our polycrystalline samples[11] give $p \sim 4\times10^{19}$ cm^{-3}. We found that the far-infrared reflectivity of the free-electron gas tends to increase at the lowest energies by increasing the scattering time. Therefore, we can conclude that the measured reflectance at 100 cm^{-1} is higher than the reflectance calculated by assuming $CrSi_2$ as totally transparent because at this energy the free-carrier tail begins to appear.

In Fig. 4 we also show n and k for the single-crystal sample, as obtained by Kramers-Kronig analysis of R. In principle, the integrals involved in the KK transformations require the knowledge of R over a very large photon energy range. In our case, it should be noticed that (i) at low energy R saturates toward 100%; (ii) we know directly the complex refractive index from 1.4 to 4.9 eV by ellipsometry. Therefore we extrapolated the reflectivity beyond the highest experimental energy ω_0 with a tail $R(\omega) = R(\omega_0)(\omega_0/\omega)^s$. The value of s was determined so that the n and k values from KK in the spectral range covered by the ellipsometer reproduce almost exactly the ellipsometric data (the largest discrepancy is 4%). We also calculated the complex dielectric function, and we analyzed the low-energy response in order to estimate the impurity concentration n_i. The plasma frequency ω_p was determined from the slope of $1/|\epsilon_1|$ vs ω^2 [see Eq. (7)]. We obtained n_i ranging from 1.25×10^{20} to 5×10^{20} cm^{-3} for $m = 0.5m_e$ and $m=2m_e$, respectively.

To assure major completeness, we examined the reflectivity of $CrSi_2$ in the far-infrared region (reported in Ref. 19) in order to obtain the optical functions n and k in the wave-number range from 200 cm^{-1} (0.0248 eV) to 400 cm^{-1} (0.0496 eV). As previously, the samples were modeled by a two-layer system ($CrSi_2/SiO_2$) on silicon. We fitted the strong vibrational peaks in R by the matrix method. The dielectric function of the $CrSi_2$ top layer was constructed with the aid of five Lorentz oscillators, by the expression

$$\tilde{\epsilon}(\omega) = \epsilon_{\infty} + \sum_{i=1}^{5} \frac{\omega_{p,i}^2}{\omega_{0,i}^2 - \omega^2 - i\gamma_i\omega}, \tag{8}$$

where $\omega_{0,i}$, $\omega_{p,i}$, and γ_i represent the energy position, the plasma energy, and the damping of the ith oscillator, respectively. The best-fit values of the parameters resulted in ϵ_{∞}=30; $\omega_{0,i}$=230, 252, 296, 352, and 370 cm^{-1}; $\omega_{p,i}$=448, 943, 545, 1182, and 768 cm^{-1}; γ_i=6.7, 9.6, 7.51, 7, and 24.8 cm^{-1}, respectively. We also calculated the transmission spectra of our multilayer system, and good agreement with the experimental spectra of Ref. 19 was found. The calculated n and k of $CrSi_2$ are shown in Fig. 5.

B. Energy bands and densities of states

The calculated band structure of $CrSi_2$ (Fig. 6) is in good agreement with the LAPW (Refs. 5 and 6) and ASW (Ref. 9) calculations. Although the space group for the C40 structure is D_6^4, which contains only half

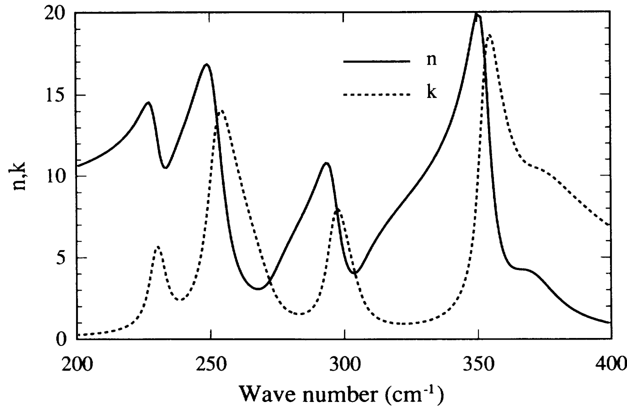

FIG. 5. Real part n and imaginary part k of the complex refractive index of $CrSi_2$ thin film in the far-infrared region, where five strong vibrational peaks appear in R (see Ref. 19).

of the full-hexagonal D_{6h} symmetry operations, Fig. 6 shows the energy bands in the irreducible part of the BZ corresponding to the D_6 point group, which is possible due to the time-reversal symmetry.[27]

The energy-band structure of $CrSi_2$ is very complicated. It builds from the 15 Cr 3d states and the 24 Si 3s,3p orbitals and extends over an energy range of about 25 eV, with low-lying bands having predominant Si 3s,3p character, which then gradually switches to Cr 3d character near E_F.[5,6] An energy gap separates the highest filled valence-band states at symmetry point L (band number $n = 21$) from the lowest empty conduction band at M ($n = 22$). Our calculated value for the indirect energy gap, $E_{\rm gap}$=0.38 eV, and the lowest-energy direct transition at L, $E_{\rm dir}$=0.47 eV, are slightly larger than those calculated with the LAPW method ($E_{\rm gap}^{\rm LAPW}$=0.30 eV, $E_{\rm dir}^{\rm LAPW}$=0.45 eV) (Ref. 6) and somewhat larger than the ASW values ($E_{\rm gap}^{\rm ASW}$=0.21 eV, $E_{\rm dir}^{\rm ASW}$=0.39 eV).[9] The discrepancy may either be due to the spherical averaging of the potentials in the LMTO and ASW methods, which is not performed in the LAPW method, or to the different exchange-correlation (XC) potentials used in the three calculations. In the LAPW calculations the Wigner interpolation formula[6] was used. In Ref. 9 no information about the XC potential was given and in our calculations we used the Barth-Hedin XC potential.[10] The ratio of the atomic-sphere radii of Cr and Si, $r = R_{\rm Cr}/R_{\rm Si}$, was 1.1 in our calculations and 1.2 in Ref. 9.

The total and partial densities of states (DOS's) are presented in Fig. 7. The total spectrum contains the contribution from all nine atoms of the unit cell. The s electrons of silicon are located near the bottom of the valence band, whereas the p states of silicon in the occupied part of the valence band are strongly hybridized with the d states of chromium. The conduction band consists of the d states of chromium mixed with the silicon p states. The f states of chromium and d states of silicon are mainly situated far above the Fermi level.

Figure 8 shows the energy-band structure of $CrSi_2$ on an expanded energy scale near the energy gap.

C. Calculated optical properties and comparison with experiment

In our theoretical investigation we calculated directly the imaginary part of dielectric function by Eq. (1) in

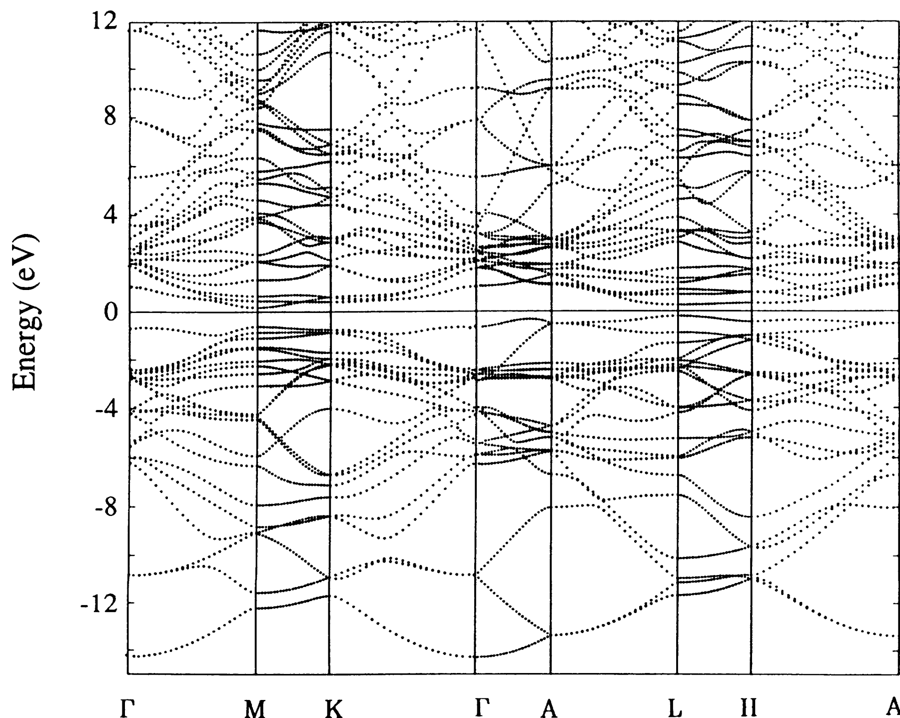

FIG. 6. Self-consistent energy-band structure of $CrSi_2$ along some symmetry lines in the Brillouin zone shown in Fig. 1.

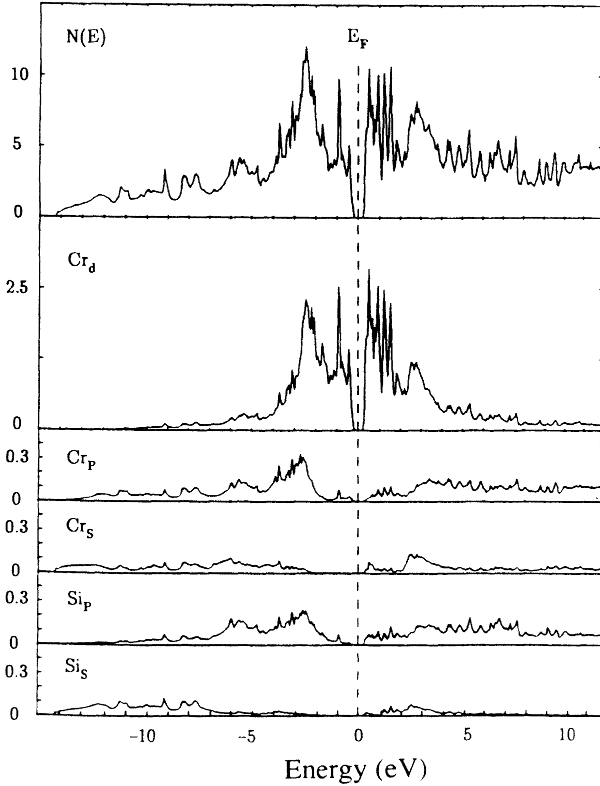

FIG. 7. Self-consistent total density of states $N(E)$ and Cr s, p, d and Si s and p partial densities of states. Units are number of states/(cell eV) and number of states/(atom eV), respectively.

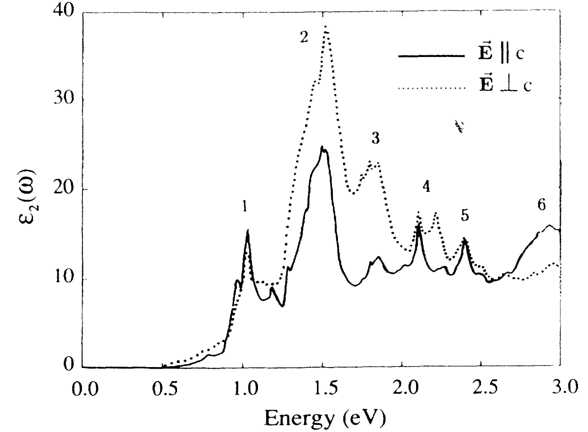

FIG. 9. The calculated imaginary part ϵ_2 of the dielectric function of $CrSi_2$. Full line is for $\mathbf{E} \parallel \mathbf{c}$ and dotted line is for $\mathbf{E} \perp \mathbf{c}$.

the wide energy range from 0 to 17 eV. The real part of the dielectric function and the reflectivity were calculated using the formulas presented above.

The $\epsilon_2(\omega)$ can be interpreted in terms of interband transitions. Figure 9 shows the calculated $\epsilon_2(\omega)$ of $CrSi_2$ for two different light polarizations $\mathbf{E} \parallel \mathbf{c}$ and $\mathbf{E} \perp \mathbf{c}$ in the energy range up to 3 eV. We limited our theoretical analysis to this range because of the large number of the interband transitions above this energy range. The anisotropy of the optical properties of $CrSi_2$ is not as strong as in WSi_2 (Ref. 21) and Pd_2Si.[28] There are six maxima in $\epsilon_2(\omega)$ in the energy range from 0 to 3 eV. All these peaks are formed from the same interband transitions for both polarizations. The difference in intensity for the two polarizations is due to the transition matrix element. We inferred from the partial densities of states that the interband transitions below 5 eV are due to the excitations of d electrons of chromium and p electrons of silicon to the conduction band. The latter has primarily d character of Cr with a small admixture of the p and f states of Cr and p and d states of Si. The experimentally obtained optical transitions begin at about 0.36 eV. This value is in good agreement with the calculated indirect energy gap E_{gap}=0.38 eV.

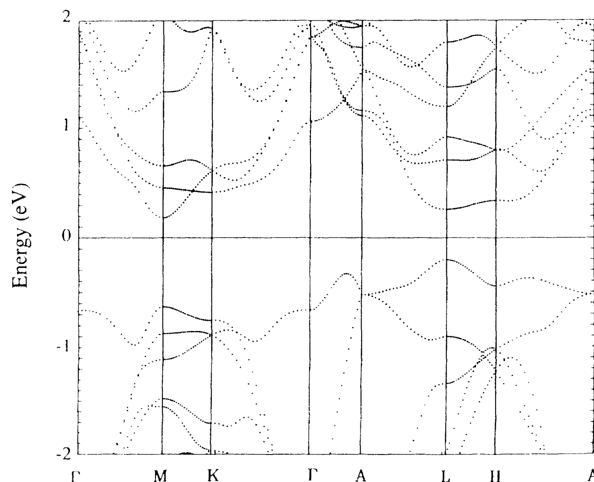

FIG. 8. Self-consistent energy-band structure of $CrSi_2$ along the high-symmetry directions near the energy gap.

We shall now give a detailed description of the main maxima of $\epsilon_2(\omega)$ (Fig. 9) in terms of the contributing interband transitions. According to the present results, the lowest direct transitions (0.47 eV) occur at the L point and involve states with L_3 (valence-band) and L_1 (conduction-band) symmetry. The first maximum at about 1 eV is due to interband transitions along the M-K symmetry direction between two nearly parallel energy bands—the 21st valence band and the conduction band, which has number 23 at the M point and number 22 at the K point due to the band crossing in this direction. The 21st valence band has the orbital character $\mathrm{Cr}(z, yz, xy, x^2-y^2, 3z^2-r^2)$ and $\mathrm{Si}(s, y, z, 3z^2-r^2, xz)$ at the M point and $\mathrm{Cr}(x, y, xz, yz, xy, x^2-y^2)$ and $\mathrm{Si}(x, y, 3z^2-r^2)$ at the K point. The character of the 23rd band is $\mathrm{Cr}(s, 3z^2-r^2, x^2-y^2, xy, xz)$ and $\mathrm{Si}(z)$ at the M point and the 22nd band is $\mathrm{Cr}(x, xz, yz, xy, x^2-y^2, 3z^2-r^2)$ and $\mathrm{Si}(x, y, z)$ at the K point. The 21→22 transitions have the contributions from the following matrix elements: $\langle z|z|3z^2-r^2\rangle$, $\langle z|z|s\rangle$, $\langle z|x|xz\rangle$ on the Cr site and $\langle s|z|z\rangle$, $\langle 3z^2-r^2|z|z\rangle$, $\langle xz|x|z\rangle$ on the Si at the M point and $\langle x|z|xz\rangle$, $\langle x|y|xy\rangle$, $\langle x|x|x^2-y^2\rangle$, $\langle x|x|3z^2-r^2\rangle$,

$\langle y|z|yz\rangle$, $\langle y|x|xy\rangle$, $\langle y|y|x^2-y^2\rangle$, $\langle y|y|3z^2-r^2\rangle$, $\langle xz|z|x\rangle$, $\langle xy|x|y\rangle$, $\langle x^2-y^2|x|x\rangle$ on Cr, $\langle 3z^2-r^2|x|x\rangle$, $\langle 3z^2-r^2|y|y\rangle$, $\langle 3z^2-r^2|z|z\rangle$ on the Si site at the K point. Therefore, this maximum is manifested for both polarizations.

The energy shoulder at ~0.78 eV comes from the 21→22 interband transitions in the vicinity of the M and H points. The most intensive maximum at 1.5 eV is due to 20→22,23 and 21→24 interband transitions along the M-K symmetry direction. The main contribution comes from the 21→24 interband transitions in the vicinity of the K point and the symmetry directions $K \to \Gamma$ and $K \to M$ close to the K point. The difference in intensity for the two polarizations is due to the transition matrix elements. The 24th energy band has the orbital character Cr($x, y, z, 3z^2-r^2, yz, xz$) and Si($s, x, y, z, x^2-y^2, 3z^2-r^2$) at the K point and the contribution to the 21→24 interband transitions comes from the matrix elements $\langle x|x|3z^2-r^2\rangle$, $\langle x|z|xz\rangle$, $\langle y|y|3z^2-r^2\rangle$, $\langle y|z|yz\rangle$, $\langle xz|z|x\rangle$, $\langle xz|x|z\rangle$, $\langle yz|z|y\rangle$, $\langle yz|y|z\rangle$, $\langle xy|y|x\rangle$, $\langle xy|x|y\rangle$, $\langle x^2-y^2|x|x\rangle$, $\langle x^2-y^2|y|y\rangle$ on Cr and $\langle x|x|s\rangle$, $\langle y|y|s\rangle$, $\langle 3z^2-r^2|x|x\rangle$, $\langle 3z^2-r^2|y|y\rangle$, $\langle 3z^2-r^2|z|z\rangle$, $\langle x|x|x^2-y^2\rangle$, $\langle y|y|x^2-y^2\rangle$, $\langle x|x|3z^2-r^2\rangle$, $\langle y|y|3z^2-r^2\rangle$ on the Si site. It can be seen that the optical transitions with the $\langle i|x,y|f\rangle$ matrix elements prevail over the $\langle i|z|f\rangle$ transitions. A numerical estimate shows that the intensity of the 21→24 transitions is seven times weaker for the $\mathbf{E} \parallel \mathbf{c}$ polarization than for the $\mathbf{E} \perp \mathbf{c}$ polarization. The third maximum comes from the superposition of 18→22, 19→23, 20→24, and 21→ 25,26 interband transitions. This maximum also has predominantly $\langle i|x,y|f\rangle$ character. The double peak at ~2.1–2.2 eV is due to the 18→23, 19→24, and 20→25 interband transitions. The fine-structure number 5, which has the same size for both polarizations, is formed by several interband transitions: 17→23,24; 18→24; 19→25; 20→26, and 21→27. The last broad 6th maximum is also formed by multiband transitions in a broad area of $\mathbf{k}$ space (14→22,23; 16→23,24; 17→ 24; 18→25; 19→26; 20→27; and 21→28 interband transitions).

We shall now compare the theoretical results with the experimental data. The anisotropy of the optical properties of $CrSi_2$ is not large, therefore we compare only the calculated optical properties for $\mathbf{E} \perp \mathbf{c}$ (Figs. 10–12). The unpolarized reflectivity $R(\omega)$ of the polycrystalline sample is shown in Fig. 10 (as the transparence region is concerned, R has been obtained from the n and k values of Fig. 4). The experimental spectrum has two structures near 0.5 and 1.1 eV. The theoretical spectrum also has two shoulders, but their positions are displaced with respect to the experimental ones.

The same situation happens in the case of the imaginary and real parts of the dielectric function. The spectrum of $\epsilon_2(\omega)$ in the film has two maxima at ~0.6 and 1.1 eV. The corresponding theoretical values are equal to ~1.0 and 1.5 eV. Although the theoretically estimated energy gap in $CrSi_2$ is in agreement with the experimental value ($E_{\text{gap}}^{\text{theor}}$=0.38 eV, $E_{\text{gap}}^{\text{expt}} \leq$0.36 eV), the theory overestimates the energy of the interband transitions beyond the gap. Figure 11 shows the $\epsilon_2(\omega)$ experimental spectra for the film samples in comparison with the the-

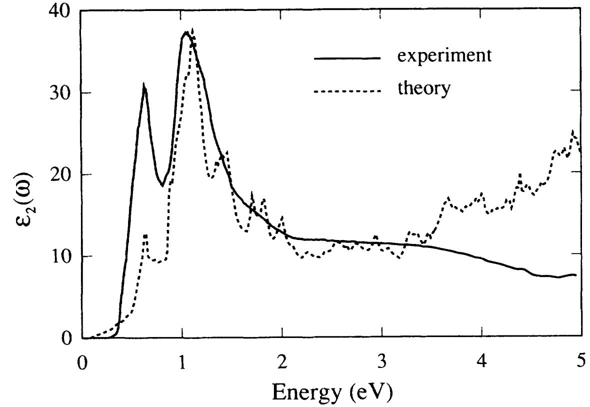

FIG. 11. Comparison between the experimental (full line) and the calculated (dotted line) imaginary part ϵ_2 of the dielectric function of $CrSi_2$. The calculated curve was shifted by 0.4 eV to lower energies.

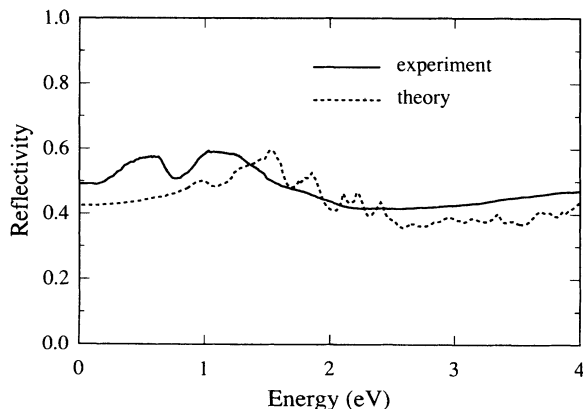

FIG. 10. Comparison between the experimental (full line) and the theoretical (dotted line) reflectivity curves of $CrSi_2$. The experimental reflectivity was obtained from n and k for the film shown in Fig. 4.

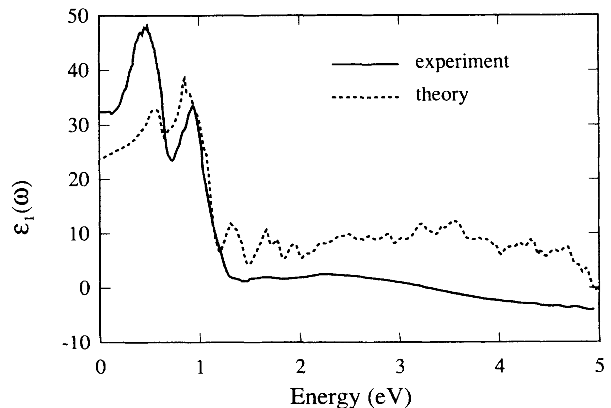

FIG. 12. Comparison between the experimental (full line) and the calculated (dotted line) real part ϵ_1 of the dielectric function of $CrSi_2$. The calculated curve was shifted by 0.4 eV to lower energies.

oretical data, which have been shifted by 0.4 eV to lower energies [the calculated $\epsilon_2(\omega)$ in Ref. 9 has the maximum at ~1.3 eV which is 0.2 eV lower than our value]. Also the theoretical $\epsilon_1(\omega)$, after a shift of 0.4 eV to lower energies, is in rather good agreement with the experiment regarding the position of the two main maxima (Fig. 12). There is no simple explanation for this disagreement. One can anticipate three sources of errors. (1) In our calculations we used the self-consistent LMTO method in the ASA approximation. The non-muffin-tin corrections to the crystalline charge density and the potential which have been neglected might be important. (2) The theoretical data are compared with measurements on a $CrSi_2$ film. A direct comparison with measurements on a bulk sample is problematic due to the presence of impurities in the crystals, which leads to metallic behavior of the optical properties in the infrared region. As was shown earlier,[6] the calculated $CrSi_2$ band gap is extremely sensitive to the near-neighbor coordination geometry and the long-range stacking sequence of $CrSi_2$ layers. The energy gap varies by ~0.1 eV for Si position changes of $\pm 0.01c$. One may expect similar sensitivity of the optical interband transition energy passing from the film to the ideal bulk (nondoped), due to subtle structural variations. (3) The main reason for the discrepancy may well be the local-density approximation. The formalism of the density-functional theory (DFT) (Ref. 7) is in principle exact for the ground-state properties (total energy, pressure, cohesive energy, etc.). However, even for the exact DFT the one-particle spectrum of the noninteracting reference system may differ from the spectrum of the actual one-electron excitations (OEE) in a solid, obtained in the optical measurements. The OEE spectrum, defined by the poles of the one-particle Green function, is given by the Dyson-type equation containing the self-energy operator $\Sigma_{xc}(\mathbf{r}, \mathbf{r}', E)$ instead of the local exchange-correlation potential $V_{xc}(\mathbf{r})$ in DFT. The self-energy operator is nonlocal, i.e., it depends on both $\mathbf{r}$ and $\mathbf{r}'$, and is also energy dependent. However, in metals the screening of the exchange interaction makes Σ_{xc} more local (more short range) and for a homogeneous electron gas the renormalization of the spectrum in the vicinity of E_F is strongly suppressed, i.e., of the order of a few percent.[29] Therefore, the DFT spectrum in metals often turns out to be very close to the OEE spectrum near E_F. For the energies far above and below E_F, the DFT spectrum can differ appreciably from the OEE spectrum. In particular, the dependence of Σ_{xc} on energy adds a complex part to the one-electron energy, with the consequent damping of the OEE spectrum, which is absent in DFT. The last effect can explain the discrepancy between the theoretically calculated $\epsilon_2(\omega)$ and experimental data at $\omega > 3.5$ eV. In this region the theory predicts strong interband transitions (see Fig. 11 in this paper and Fig. 3 in Ref. 9), which are absent in the experiment. This is confirmed both by many-particle calculations (see Refs. 30–32) and by comparison with experimental data. The discrepancy is usually less than 10%. The situation is different in insulating crystals. The DFT usually underestimates the dielectric gap[8] while many-body perturbation theory gives quite reasonable results for the gap.[33–35]

In the present case, the DFT reproduces the energy gap in $CrSi_2$ in excellent agreement with the experiment. As discussed previously,[5,6] the states around the gap have predominantly Cr 3*d* character. Therefore, the state dependence of the self-energy should be small within this group of bands, and the band gap is accurately represented by the LDA potential.[36] This condition is not fulfilled for the rest of the energy bands originating from the Cr states hybridized with Si 3*s* and 3*p* states. The DFT cannot reproduce the energies of the optical interband transitions beyond the gap. In the case of $CrSi_2$ the DFT overestimates the interband transitions, although, in most other cases, the DFT underestimates the dielectric gap. There is, however, no rigorous theorem that DFT always should underestimate the gap.

IV. CONCLUSIONS

In conclusion, the band-structure calculations and the experimental data of the optical properties of $CrSi_2$ provide further evidence that $CrSi_2$ is an ordinary band-type semiconductor with a small indirect energy gap. The anisotropy of the optical properties of $CrSi_2$ is not large. The calculated band gap is in good agreement with the measured optical value. The calculated and measured reflectance, $\epsilon_2(\omega)$ and $\epsilon_1(\omega)$, are in excellent agreement after a downward shift of the calculated curves by 0.4 eV. The predicted strong interband transitions at 5 eV are absent in the experiment.

ACKNOWLEDGMENTS

We are grateful to O. Gunnarsson for a critical reading of the manuscript and for several useful suggestions. One of us (V.N.A.) thanks Barry M. Klein for the helpful discussion on the energy-gap problem in $CrSi_2$. This work was partially supported by Progetto Finalizzato "Materiali e Dispositivi per Elettronica a Stato Solido" and by Gruppo Nazionale Struttura della Materia del Consiglio Nazionale delle Ricerche, Italy. The authors acknowledge Professor F. Lévy of the Ecole Polytechnique Fédérale de Lausanne, who grew and made available the single-crystal samples. Two of us (V.N.A. and V.N.A.) would like to thank the MPI FKF for hospitality during their stay in Stuttgart.

*Permanent address: Institute of Metal Physics, Ukrainian Academy of Sciences, Vernadskogo 36, 252142 Kiev, Ukraine.

[1]S.P. Murarka, in *Microelectronic Materials and Processes*, edited by R.A. Levy (Kluwer Academic, Dordrecht, 1989).
[2]L.J. Chen and K.N. Tu, Mater. Sci. Rep. **6**, 53 (1991).
[3]M.C. Bost and J.E. Mahan, J. Appl. Phys. **63**, 839 (1988).
[4]A. Franciosi, J.H. Weaver, D.G. O'Neill, F.A. Schmidt, O.

Bisi, and C. Calandra, Phys. Rev. B **28**, 7000 (1983).

[5]L.F. Mattheiss, Phys. Rev. B **43**, 1863 (1991).

[6]L.F. Mattheiss, Phys. Rev. B **43**, 12 549 (1991).

[7]P. Hohenberg and W. Kohn, Phys. Rev. **136**, B964 (1964); W. Kohn and L.J. Sham, *ibid.* **140**, A1133 (1965).

[8]L.J. Sham and M. Schluter, Phys. Rev. Lett. **51**, 1888 (1983); Phys. Rev. B **32**, 3883 (1985).

[9]M.P.C. Krijn and R. Eppenda, Phys. Rev. B **44**, 9042 (1991).

[10]U. von Barth and L. Hedin, J. Phys. C **4**, 2064 (1971).

[11]F. Nava, T. Tien, and K.N. Tu, J. Appl. Phys. **57**, 2018 (1985).

[12]C.J. Bradley and A.P. Cracknell, *The Mathematical Theory of Symmetry in Solids* (Clarendon, Oxford, 1972).

[13]M. Hansen and K. Anderko, *Constitution of Binary Alloys* (McGraw-Hill, New York, 1958), p. 560.

[14]K.N. Mason, Prog. Cryst. Growth Charact. **2**, 269 (1979).

[15]O.K. Andersen, Phys. Rev. B **12**, 3060 (1975).

[16]H.L. Skriver, *The LMTO Method* (Springer, Berlin, 1984).

[17]O. Jepsen and O.K. Andersen, Solid State Commun. **9**, 1763 (1971).

[18]H. Ehrenreich and M.H. Cohen, Phys. Rev. **115**, 786 (1959).

[19]A. Borghesi, A. Piaggi, A. Franchini, G. Guizzetti, F. Nava, and G. Santoro, Europhys. Lett. **11**, 61 (1990).

[20]O.S. Heavens, *Optical Properties of Thin Solid Films* (Butterworths, London, 1955), p. 69.

[21]V.N. Antonov, Vl.N. Antonov, O. Jepsen, O.K. Andersen, A. Borghesi, C. Bosio, F. Marabelli, A. Piaggi, G. Guizzetti, and F. Nava, Phys. Rev. B **44**, 8437 (1991).

[22]H.R. Philipp, in *Handbook of Optical Constants of Solids*, edited by E.D. Palik (Academic, Orlando, 1985), p. 749.

[23]D.F. Edwards, in *Handbook of Optical Constants of Solids*, edited by E.D. Palik (Academic, Orlando, 1985), p. 547.

[24]J.M. Bennet and M.J. Booty, Appl. Opt. **5**,41 (1966).

[25]J.E. Nestell, Jr. and R.V. Christy, Appl. Opt. **11**, 643 (1972).

[26]M. Amiotti, A. Borghesi, F. Marabelli, A. Piaggi, G. Guizzetti, and F. Nava, Appl. Surf. Sci. **53**, 230 (1991).

[27]M. Lax, *Symmetry Principles in Solid State and Molecular Physics* (Wiley, New York, 1974).

[28]M. Amiotti, G. Guizzetti, F. Marabelli, A. Piaggi, V.N. Antonov, Vl.N. Antonov, O. Jepsen, O.K. Andersen, A. Borghesi, F. Nava, V.V. Nemoshkalenko, R. Madar, and A. Rouault, Phys. Rev. B **45**, 13 285 (1992).

[29]L. Hedin and S. Lundqvist, in *Solid State Physics*, edited by H. Ehrenreich and D. Turnbull (Academic, New York, 1969), Vol. 23, p. 1.

[30]L. Hedin, Phys. Rev. A **139**, 796 (1965).

[31]A.H. MacDonald, J. Phys. F **10**, 1737 (1980).

[32]M. Schreiber and U. Bross, J. Phys. F **13**, 1895 (1983).

[33]W.E. Picket and C.S. Wang, Phys. Rev. B **30**, 4719 (1984).

[34]G. Strinati, H.G. Mattausch, and W. Hanke, Phys. Rev. B **25**, 2667 (1982).

[35]M.S. Hybertsen and S.G. Louie, Phys. Rev. B **34**, 5390 (1986).

[36]O. Jones and O. Gunnarsson, Phys. Rev. Lett. **55**, 107 (1985).